Detachment and diffusive-convective transport in an evolving heterogeneous two-dimensional biofilm hybrid model

E. Luna, G. Domínguez-Zacarias, C. Pio Ferreira, and J. X. Velasco-Hernandez
Instituto Mexicano del Petróleo, D.F. 07730, Mexico
(Received 29 July 2004; published 20 December 2004)

Under the hypothesis of correlation between biofilm survival and nutrient availability, by considering fluid drag forces and mortality due to nutrient depletion, a biofilm detachment/breaking condition is derived. The mechanisms leading to biofilm detachment/breaking are discussed. We construct and describe a hybrid model for a heterogeneous biofilm attached to walls in a channel where liquid is flowing. The model is called hybrid because it couples conservation equations with a cellular automaton. The biofilm layer is viewed as a porous medium with variable porosity, tortuosity, and permeability. The model is solved using asymptotic and finite differences methods. Results for porosity, nutrient distribution, and average surface location are presented. The model is capable of reproducing biofilm heterogeneity as well as the typical surface fingering (mushroomlike structure).

DOI: 10.1103/PhysRevE.70.061909 PACS number(s): 87.17.Aa, 87.18.Bb, 87.17.Ee, 83.85.Pt

I. INTRODUCTION

As defined by Donlan [1] a biofilm is an assemblage of surface-associated microbial cells that is enclosed in an extracellular polymeric substance matrix. Biofilms play important and diverse roles in many areas of applied science and technology such as oil enhanced recovery and transportation, pharmaceutical research, food processing, medical devices, antibiotic resistance, electrochemical corrosion, waste water treatment, and others [2]. In this work, we present a model for the interaction of fluid flow and biofilm internal structure. Our aim is to explore plausible mechanisms for biofilm persistence and eventual detachment based on the interaction between fluid flow, the spatial structure of microbial communities, and transport of nutrients. To achieve this aim we have constructed a hybrid mathematical model. In areas such as the study of antimicrobial resistance and microbial enhanced corrosion (MIC), biofilms are known for being difficult to eradicate [2,3] given their ability for evolving resistance against biocides, antibiotics and, in fact, against every single antimicrobial substance applied to them. Using the model presented in this work we would like to predict the time to maximal biofilm growth, the time to biofilm detachment and, ultimately, we would like to use the model to predict optimal dosages of biocides or antibiotics to prevent the development of resistance and hence biofilm destruction and to predict the onset of pitting in the case of MIC. This last objective is still beyond the model we describe here but research is under way that addresses this problem and that will be published elsewhere. In particular we explore here the processes of biofilm detachment, bulk flow through the system, diffusive and convective transport of nutrients, and biofilm growth. As pointed out by Stewart *et al.* [2] engineering biofilm control is a formidable task because the interaction of biofilm with its environment involves very complex processes at the cellular, physicochemical, genetically, and physical levels of interaction. Mathematical models can be considered methodological tools for the study of complex systems since they allow us to organize and integrate the diverse phenomena occurring in a biofilm in a systematic and efficient way. The predictive and explanatory capacity of a well-formulated model is invaluable for the study of this kind of complex phenomena. The model presented here is an attempt to do this.

Classical mathematical models for biofilm structure and dynamics are mainly one dimensional [4–8]. This simplification, although natural and justifiable in certain situations, is clearly insufficient to describe the heterogeneous nature of microbial communities both at the surface as well as internal levels [9]. Recently, several multidimensional models have appeared that have been used to successfully explore both structural and dynamic behaviors of real biofilms [7,10–16]. These multidimensional models are based on cellular automata and/or continuum conservation equations. Roughly speaking, these are hybrid models where conservation for momentum (Navier–Stokes or Darcy's law) and species equations are solved in the surrounding fluid as well as in the bacterial layer seen as a solid or a homogeneous porous medium. Another important area of research has been the study of the internal biofilm morphology. In this area we can cite the work of Hermanowicz *et al.* [17], reporting that multifractal internal structure varies with the geometric scale and that there exists, possibly, a relationship between anisotropic morphology and flow direction.

In our work, the conservation equations are used to compute nutrient distributions and the velocity field; a cellular automaton (CA) simulates the growth of the bacterial colony. Biofilm internal structure is viewed as a porous medium with variable properties in space and time. Beer and Stoodley [18] modeled nutrient transport into the biofilm assuming it to be a porous media with constant properties. By contrast, in our model porosity is variable and is updated at discrete time steps from the colonization mean values produced by the CA; tortuosity and permeability are deduced from theoretical and empirical relationships, respectively, following the results of Islas-Juarez [19] and Cussler [20]. The CA simulates the evolution of the bacterial community's spatial structure based in cell division, space competition, and substrate concentrations. Within the biofilm, Darcy's law, mass conserva-

 ©2004 The American Physical Society

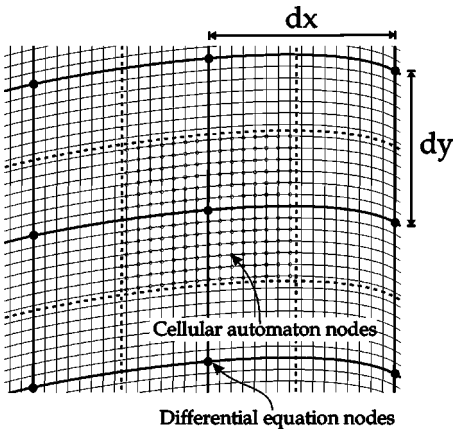

FIG. 1. Grids used for the discrete and continuous model.

tion, and species balance equations (all of them dynamic properties) are used to compute pressure, velocity, and nutrient distribution. Under a certain hypothesis, stated in the next section, on the bulk fluid outside the biofilm, the Navier–Stokes and species conservation equations were simplified to a perturbed Poiseuille flow and a constant concentration solution. Using all of these assumptions our two-dimensional model is capable of reproducing biofilm internal heterogeneities, biofilm surface behavior, nutrient penetration, and biofilm critical point of rupture or detachment. Results for porosity, nutrient distribution, average surface location, and rupture times are presented.

II. CONTINUOUS AND DISCRETE MODEL IN THE BACTERIAL BIOFILM

In this section we present some methodological considerations about coupling continuous and discrete formalism for a bacterial biofilm. After that, those ideas are applied to a particular case. In the model overview presented in the Introduction we indicated that biofilm behavior is modeled with a CA while the nutrient distribution and fluid dynamics are described with a continuous model. The conservation equations and the CA are coupled through porosity, permeability, tortuosity, biofilm-fluid interface position, concentration, and rate consumption of nutrients.

Given the hybrid nature of our model we used two coupled grids for the computer implementation: one for the CA and another for the conservation equations. In both cases the grid size was carefully chosen for consistency with the definition of porous media, where the characteristic porous length, the bacterial size, must be very small compared to a control volume in the continuum formulation. Our scheme allowed us to have up to 50×50 CA grid nodes in each continuum control volume (see Fig. 1).

The algorithm for our computer implementation is shown schematically in Fig. 2. The simulation begins with an initial random bacterial distribution to generate the initial values for porosity (ϕ), permeability (k), tortuosity (τ), interface position (Γ), and nutrient rate consumption (A). Using these variables the conservation equations compute the nutrient distribution in the biofilm (Y_f). Once this is done, the nutrient

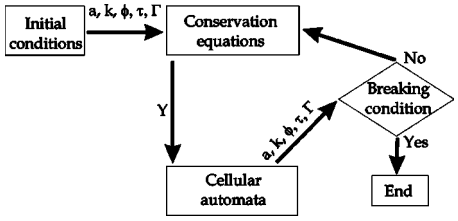

FIG. 2. Schematic procedure for solving the hybrid model.

concentration is used by the CA and new porosity, permeability, tortuosity, and interface values are generated. This cycle is repeated until the final time is reached or a breaking condition is satisfied. This rupture condition is derived from considerations on biofilm mechanical resistance and stresses induced by the fluid drag.

III. MODEL DESCRIPTION

Our model describes the interaction of fluid dynamics, nutrients distribution, and biofilm internal structure. However, in order to derive our model we considered the large-scale problem of fluid flow in a channel where the biofilm is an obstacle. Given the small dimensions of biofilms compared to the diameter of an oil pipe or even a catheter in medical applications, the effect of a biofilm patch on the velocity profile of a fluid is hardly of relevance. We present it here because it is useful, in our opinion, to keep track of the multiple spatial and temporal scales involved in the biofilm-fluid interaction.

At the larger spatial scale, the physical model consists of a fluid flowing between two parallel plates separated by a distance $2h$, length L, with $L \gg h$, and infinite depth to simulate an effective two-dimensional system. The fluid of viscosity μ and flow rate Q is carrying nutrients with concentration Y_f. A bacterial biofilm with surface $\Gamma(x,t) \ll h$ grows attached to the plates surface, where the coordinate system (x,y) is shown in Fig. 3.

To simplify the free flow problem we specify the following:

(i) in $y=h$ there exists symmetrical planes; this approximation is valid when $\Gamma \ll h$; (ii) the fluid velocity into the bacterial film (porous medium) is very small compared with the free flow mean velocity.

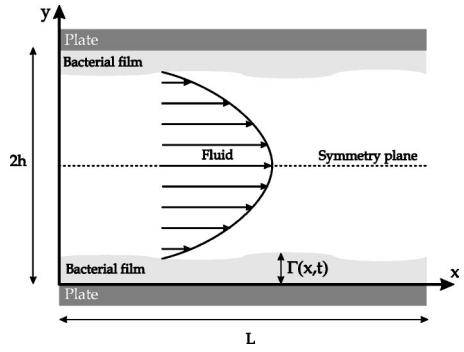

FIG. 3. Physical model to study.

Using the above assumptions the flux between the channel walls and the porous layer can be modeled as a perturbed Poiseuille flow with velocity $u_p(x,y,t)$ and pressure $p_f(x)$ given by

$$u_p = \frac{3}{4}\frac{Q}{h-\Gamma}\left[1-\frac{(h-y)^2}{(h-\Gamma)^2}\right] \text{ and } p_f = p_0 - \frac{3}{2}Q\mu\int_0^x \frac{dx'}{(h-\Gamma)^3}, \tag{1}$$

where p_0 is the pressure at $(x=0)$. Note that the order of magnitude of the characteristic substrate-concentration variations (ΔY_f) along the channel can be obtained by comparing of the convective substrate flux along the longitudinal direction $[Q\Delta Y_f/(hL)]$ and the diffusive ingoing fluxes in the transversal direction (J_b/h), where J_b is the characteristic substrate consumption rate within the biofilm. Therefore we postulate that

$$\Delta Y_f \sim \frac{LJ_b}{Q} \ll 1, \tag{2}$$

and then the concentration along the duct can be considered constant $Y(x,y,t)=Y_f$ implying that the fluid is always carrying the original substrate concentration.

IV. POROUS FLOW

Within the biofilm the mass conservation equation for variable porosity is given by

$$\frac{\partial}{\partial t}[\phi\rho + (1-\phi)\rho_b] + \vec{\nabla}\cdot(\rho\vec{u}) = 0, \tag{3}$$

where ρ and ρ_b are the fluid and bacterial mass densities, respectively, and $\vec{u}=u\hat{x}+v\hat{y}$ is the velocity vector. The relationship between velocities and pressure is governed by Darcy's law:

$$u = -\frac{k}{\mu}\frac{\partial p}{\partial x} \quad \text{and } v = -\frac{k}{\mu}\frac{\partial p}{\partial y}. \tag{4}$$

The mass nutrient fraction Y is governed by the species balance equation for variable porosity and low velocities where dispersion effects are neglected:

$$\phi\frac{\partial Y}{\partial t} + \vec{u}\cdot\vec{\nabla}Y = \nabla\cdot(\phi D_\phi \nabla Y) + A, \tag{5}$$

where A is the substrate consumption rate, and D_ϕ is the effective molecular diffusion coefficient of nutrients in the fluid. The relationship $D_\phi = D/\tau$ is used, where D is the free molecular diffusion coefficient. It is assumed that tortuosity is related to porosity by the formula derived by Islas-Juarez [18] and Cussler [19]:

$$\tau = 1 + \frac{\alpha^2(1-\phi)^2}{\phi}. \tag{6}$$

This relationship is based on a brick arrangement geometric model where α is an adjustment parameter related to the mean brick aspect ratio. Permeability can be calculated using [21]

$$k = \frac{r_b^2}{16(1-\phi)^{3/2}[1+64(1-\phi)^3]}, \tag{7}$$

where r_b is the average bacterial radius. This empirical model was obtained for a fibrous medium but it works very successfully for random beds of ellipsoids [22] that correspond to the bacterial model that we use in this work.

A. Initial and boundary conditions

To solve Eqs. (3)–(5) it is necessary to specify initial and boundary conditions. Initially there is a known substrate concentration inside the biofilm $Y(x,y,t=0)=Y_{ini}$. The initial biofilm profile $\Gamma(x,t=0)$ is defined as [23]

$$\Gamma(x,t=0) = \tilde{\Gamma}_0 + \hat{\Gamma}_0 \sin(k_\Gamma x). \tag{8}$$

Here, $\tilde{\Gamma}_0$ is the profile average value, $\hat{\Gamma}_0$ and k_Γ represent the amplitude and wave number of a small sinusoidal perturbation, respectively. The initial porosity $\phi(x,y,t=0)$ is generated sorting occupancy in the automaton grid and using the expression

$$\phi(x,y,t=0) = \phi_{\min} + \frac{N_0}{N_T}(1-\phi_{\min}) \tag{9}$$

in each control volume below the interface $\Gamma(x,t=0)$, where $\phi_{\min}$ is the minimum porosity that the bacterial film can reach, N_0 and N_T are empty and total sites in the control volume used to compute porosity, respectively. This procedure to calculate porosity is always used but bacterial occupancy is obtained from the CA. Once the porosity is calculated, Eqs. (6) and (7) give the values for tortuosity and permeability.

It is assumed that $x=0$, $x=L$, and $y=0$ are impermeable barriers, so that the boundary conditions for pressure and nutrient concentration are

$$\left[\frac{\partial p}{\partial x}\right]_{x=0,L} = \left[\frac{\partial Y}{\partial x}\right]_{x=0,L} = \left[\frac{\partial p}{\partial y}\right]_{y=0} = \left[\frac{\partial Y}{\partial y}\right]_{y=0} = 0. \tag{10}$$

On $\Gamma(x,t)$ the pressure and nutrient concentration must be continuous functions, therefore

$$p(x,y=\Gamma,t) = p_0 - \frac{3}{2}Q\mu\int_0^x \frac{dx'}{(h-\Gamma)^3} \text{ and } Y(x,y=\Gamma,t) = Y_f. \tag{11}$$

B. Dimensionless equations

Equations (3)–(7) and boundary conditions (8)–(11) can be put in dimensionless form using $x^*=x/L$, $y^*=y/\tilde{\Gamma}_0$, $t^*=t/t_{CB}$, $Y^*=Y/Y_f$, $\gamma=\Gamma/\tilde{\Gamma}_0$, $k^*=k/r_b^2$, $a=A\tilde{\Gamma}_0^2/(DY_f)$, and $p^*=2h^3(p_0-p)/(3\mu QL)$ where t_{CB} is the average bacterial life time. Combining Darcy's law and mass conservation equations, and removing the superscript * for simplicity, the dimensionless system of equations can be written as

$$\varepsilon^2\frac{\partial k}{\partial x}\frac{\partial p}{\partial x}+\frac{\partial k}{\partial y}\frac{\partial p}{\partial y}+\varepsilon^2 k\frac{\partial^2 p}{\partial x^2}+k\frac{\partial^2 p}{\partial y^2}=-\varepsilon^2\Omega\frac{\partial \phi}{\partial t}, \quad (12)$$

$$\varsigma\phi\frac{\partial Y}{\partial t}+\varepsilon^2\beta k\frac{\partial p}{\partial x}\frac{\partial Y}{\partial x}+\beta k\frac{\partial p}{\partial y}\frac{\partial Y}{\partial y}=\Phi\left[\varepsilon^2\frac{\partial^2 Y}{\partial x^2}+\frac{\partial^2 Y}{\partial y^2}\right]+\varepsilon^2\frac{\partial \Phi}{\partial x}\frac{\partial Y}{\partial x}+\frac{\partial \Phi}{\partial y}\frac{\partial Y}{\partial y}+a, \quad (13)$$

$$\gamma(x,t=0)=1+\frac{\hat{\Gamma}_0}{\tilde{\Gamma}_0}\sin(Lk_T x), \quad Y=(x,y,t=0)=\frac{Y_{ini}}{Y_0}, \quad (14)$$

$$\left[\frac{\partial p}{\partial x}\right]_{x=0,1}=\left[\frac{\partial Y}{\partial x}\right]_{x=0,1}=\left[\frac{\partial p}{\partial y}\right]_{y=0}=\left[\frac{\partial Y}{\partial y}\right]_{y=0}=0, \quad (15)$$

$$Y(x,y=\gamma,t)=1, \quad p(x,y=\gamma,|t)=\int_0^x\frac{dx'}{(1-\gamma\delta)^3}, \quad (16)$$

where $\varepsilon=\tilde{\Gamma}_0/L$, $\beta=3r_b^2QL/(2Dh^3)$, $\varsigma=\tilde{\Gamma}_0^2/(t_{CB}D)$, $\Omega=2h^3L(\rho-\rho_b)/(3Qr_b^2t_{CB}\rho)\delta=\tilde{\Gamma}_0/h$, and $\Phi=\phi^2/[\phi+\alpha^2(1-\phi)^2]$. Here, β is the ratio of convective to diffusive substrate fluxes, ε represents the aspect ratio of the bacterial film, ς is the relationship between diffusive and bacterial life times, δ is the relative amount of the channel occupied by bacterial film, and Ω is the ratio of characteristic convection time and mean bacterial life time. Equations (12)–(16) are solved simultaneously coupled with the CA.

C. Cellular automaton

In the CA each lattice node is identified by a state that can be occupied (**1**) by a bacterium or empty (**0**) and by the nutrient concentration. The temporal evolution of the bacterial population is governed by the following local rules.

(i) Colonization (cell division). An empty node can be occupied with probability $N_eR/4$ where N_e is the number of occupied nodes in this so-called von Neumann neighborhood, and R is the probability of colonization of unoccupied sites. This can be thought of as bacterial replication. A node needs to have a minimum substratum concentration $Y_{\min}$, to be colonized by a bacteria. When a node is colonized there is an increment Δa_b in the substratum consumption rate matrix.

(ii) Mortality (competition). An occupied node can become empty with probability $N_0P/4$, where N_0 is the number of occupied nodes in this von Neumann neighborhood with P is the probability of death due to competition for space and resources. Also, the node becomes empty if the amount of substratum is less than a minimum $Y_{\min}$ to stay alive, when it occurs there is a decrement Δa_d in the substratum consumption rate matrix.

A two-dimensional lattice with periodic boundary conditions was used. The initial condition was a random distribution of 80% occupied cells in the area below $\Gamma(x,t=0)$, for $\phi_{\min}=0.20$ it produced a mean biofilm porosity of 37.3%.

V. ASYMPTOTIC AND NUMERICAL SOLUTIONS

In practical cases, the parameters defined above behave like $\varsigma\to 0$, $\Omega<1$, $\beta<1$, $\delta\ll 1$, and $\varepsilon\ll 1$. To simplify the problem we solved for the case $\varsigma=0$, since convective times are very small compared with the characteristic life time of an individual bacterium provided the temporal variation of substrate concentration can be neglected. Since $\varepsilon\ll 1$ it is possible to use an asymptotic expansion [24] for pressure and concentration in terms of powers of ε^2:

$$p=\sum_{n=0}^{\infty}p_n\varepsilon^{2n} \text{ and } Y=\sum_{n=0}^{\infty}Y_n\varepsilon^{2n}. \quad (17)$$

To order zero, the pressure and substrate concentration systems are

$$\frac{\partial k}{\partial y}\frac{\partial p_0}{\partial y}+k\frac{\partial^2 p_0}{\partial y^2}=0, \quad (18)$$

$$\beta k\frac{\partial p_0}{\partial y}\frac{\partial Y_0}{\partial y}=\Phi\frac{\partial^2 Y_0}{\partial y^2}+\frac{\partial Y_0}{\partial y}\frac{\partial \Phi}{\partial y}+a, \quad (19)$$

$$\left[\frac{\partial p_0}{\partial y}\right]_{y=0}=0, \quad p_0(x,y=\gamma,t)=\int_0^x\frac{dx'}{(1-\gamma\delta)^3}, \quad (20)$$

$$\left[\frac{\partial Y_0}{\partial y}\right]_{y=0}=0 \quad \text{and} \quad Y_0(x,y=\gamma)=1. \quad (21)$$

These equations can be integrated once to get

$$p_0(x)=\int_0^x\frac{dx'}{(1-\gamma\delta)^3}\simeq x+3\delta\int_0^x\gamma dx'$$

and

$$\frac{\partial Y_0}{\partial y}=-\frac{1}{\Phi}\int_0^y a dy'. \quad (22)$$

After the CA generates γ, ϕ, and a these equations can be solved using standard finite-difference numerical methods. To order ε^2, equations for the pressure and concentration are

$$\frac{\partial}{\partial y}\left(y\frac{\partial p_1}{\partial y}\right)=-3\delta k\frac{\partial \gamma}{\partial x}-(1+3\delta\gamma)\frac{\partial k}{\partial x}-\Omega\frac{\partial \phi}{\partial t}, \quad (23)$$

$$\frac{\partial}{\partial y}\left(\Phi\frac{\partial Y_1}{\partial y}\right)=-\frac{\partial}{\partial y}\left(\Phi\frac{\partial Y_0}{\partial x}\right)+\beta k(1+3\delta\gamma)\frac{\partial Y_0}{\partial x}+\beta k\frac{\partial p_1}{\partial y}\frac{\partial Y_0}{\partial y}, \quad (24)$$

$$\left(\frac{\partial p_1}{\partial y}\right)_{y=0} = p_1(y=\gamma)=0 \quad \text{and} \quad \left(\frac{\partial Y_1}{\partial y}\right)_{y=0} = Y_1(y=\gamma)=0. \tag{25}$$

Finally, to order ε^4, equations for the pressure and concentration are

$$\frac{\partial}{\partial y}\left(y\frac{\partial p_2}{\partial y}\right) = \frac{\partial}{\partial x}\left(k\frac{\partial p_1}{\partial x}\right), \tag{26}$$

$$\frac{\partial}{\partial y}\left(k\frac{\partial Y_2}{\partial y}\right) = -\frac{\partial}{\partial x}\left(k\frac{\partial Y_1}{\partial x}\right) + \beta k\left[(1+3\delta\gamma)\frac{\partial Y_1}{\partial x} + \frac{\partial p_1}{\partial x}\frac{\partial Y_0}{\partial x} + \frac{\partial p_1}{\partial y}\frac{\partial Y_1}{\partial y} + \frac{\partial p_2}{\partial y}\frac{\partial Y_0}{\partial y}\right], \tag{27}$$

$$\left(\frac{\partial p_2}{\partial y}\right)_{y=0} = p_2(y=\gamma)=0 \quad \text{and} \quad \left(\frac{\partial Y_2}{\partial y}\right)_{y=0} = Y_2(y=\gamma)=0. \tag{28}$$

The right-hand sides in Eqs. (22)–(28) are known functions that depend on previous orders, so they can be easily integrated numerically for each x using finite differences and three-diagonal matrixes. This solution method was selected because it has numerical advantages mainly; it is fast and does not need huge amounts of memory. The grid size used was 200×200, the programming language was FORTRAN running on a Pentium 4 machine.

VI. BREAKING CONDITION

For each x, the maximum nutrient concentration exists in the neighborhood of Γ; below the interface the nutrient concentration decreases with depth. If the biofilm grows enough the nutrient concentration may reach a critical value at the bottom of the biofilm, near the attachment interface, and the bacteria can no longer reproduce or stay alive. There are studies centered on biofilm disintegration and detachment that consider the effect of fluid flow over the biofilm surface [15,25–27]. Cellular automata have been used to study biofilm structure and detachment. In particular, Hermanowicz [28,29] used a probabilistic model for detachment using biofilm strength and hydrodynamic shear stress in a cellular automata, and Indekeu *et al.* [30] using a cellular automaton characterized the relative importance of the nutrient supply process to determine the biofilm structure.

We assume that microbial death within the biofilm weakens attachment strength and mechanical resistance properties, especially at the bacteria-plate interface. It is know that in *Pseudomonas fluorescence* forms very quickly in well-oxygenated environments but, as oxygen is depleted due to biofilm growth, biofilm disintegration develops [31]. This disintegration may be due to denaturalization of the extrapolyscaccharide (EPS) substance matrix that surrounds the biofilm. In our model we are not considering the EPS but, phenomenologically, cell death correlation with nutrient depletion and biofilm growth is a reasonable approximation to the process. It is true that, as discussed by Lewis [3], biofilm destruction due to nutrient limitation other than oxygen has not been conclusively demonstrated but it is a reasonable and it is a potentially powerful mechanism to induce biofilm destruction. Therefore, under the biologically reasonable assumption that nutrient depletion is associated with biofilm destruction, a very simple model was developed to predict the breaking point of the bacterial film. Let us assume that a section $x_b - x_a$ at the solid plate-bacteria interface loses its mechanical resistance properties due to bacterial death. To produce a rupture, the forces per unit length due to fluid drag (F_d) must be greater than a critical value that depends on the thickness and the internal structure of the biofilm (see Fig. 4).

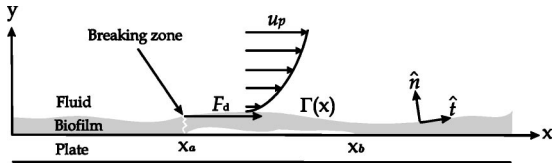

FIG. 4. Model to describe the breaking point in the biofilm.

$$|F_d| = \left|\int_{x_a}^{x_b} \mu\frac{\partial u_p}{\partial n}ds\right| > \sigma_a\Gamma(x_a), \tag{29}$$

where n and ds are the normal and differential arc surface in Γ, respectively, and σ_a is the maximum stress that the biofilm can resist. Using u_p this relationship in dimensionless form can be rewritten as (and removing the superscript *)

$$\left|\int_{x_a}^{x_b} \frac{1}{(1-\delta\gamma)^2}\sqrt{1+\varepsilon^2\left(\frac{\partial\gamma}{\partial x}\right)^2}\,dx\right| > \Pi_0\gamma(x_a), \tag{30}$$

where $\Pi_0 = 2\sigma_a\tilde{\Gamma}_0 h^2/(3Q\mu L)$ represents the ratio between drag and mechanical resistance forces.

VII. RESULTS AND DISCUSION

The numerical results presented in this section were calculated with: $\alpha=0.57$, $\delta=1\times10^{-2}$, $\Omega=1\times10^{-4}$, $\beta=1\times10^{-4}$, $\varepsilon=0.01$, $\Pi_0=0.11$ (to estimate this parameter, σ was taken from Picioreanu [15]), $\Delta a_b=0.07$, $\Delta a_d=0.04$, $Y_{\min}/Y_f=0.5$, and different values for R and P.

Heterogeneities within the biofilm are apparent in the porosity distribution. Figure 5(a) shows the porosity field within the biofilm for $t=250$, $R=0.04$, and $P=0.03$. The corresponding nutrient distribution is shown in Fig. 5(b). Note that nutrient distribution, especially near the fluid-biofilm interface, depends mainly on the bacterial layer thickness and to a minor degree on the heterogeneities in porosity, permeability, and tortuosity. It is convenient here to remind the reader that parameter R represents the likelihood of colonization of empty spaces within the biofilm, and the parameter P represents the likelihood of bacterial extinction (death) due to competition from other bacteria.

The mean thickness ($\overline{\gamma}$) evolution for ten simulations is presented in Fig. 6(a) where the bacterial life history parameters were $P=0.03$ for different values for R. The figure shows the point at which the biofilm becomes unstable and

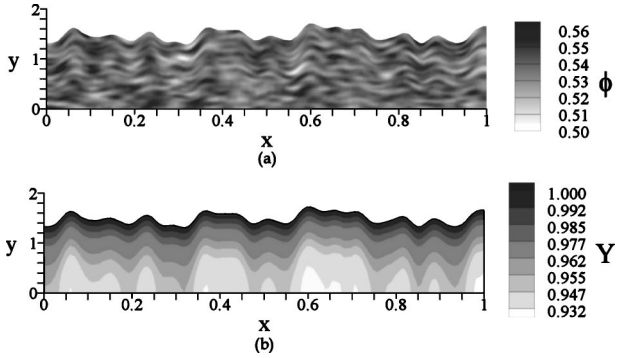

FIG. 5. (a) Porosity distribution and (b) dimensionless nutrient distribution as function of the dimensionless longitude.

detaches from the plate; at this point $\overline{\gamma}$ is wide enough to prevent nutrient diffusion and convection to the bottom of the film inducing bacterial death. It is possible to observe for small values of R that there is a transient where the bacterial surface decreases before the period of accelerated growth ensues. This behavior is consistent with the actual dynamics of bacterial and microbial growth.

Our results also show that the biofilm mean porosity evolves through time until it reaches an asymptotic value that depends on the bacteria population parameters, R and P. Figure 6(b) shows the porosity temporal evolution for $P=0.03$ and different values in R, where it can be observed that the equilibrium mean porosity value is inversely proportional to R. Just before biofilm rupture there is a pronounced increase in porosity, indicative of massive bacterial death. Thus there exists a critical time when bacteria begin to die inducing a sudden porosity increase.

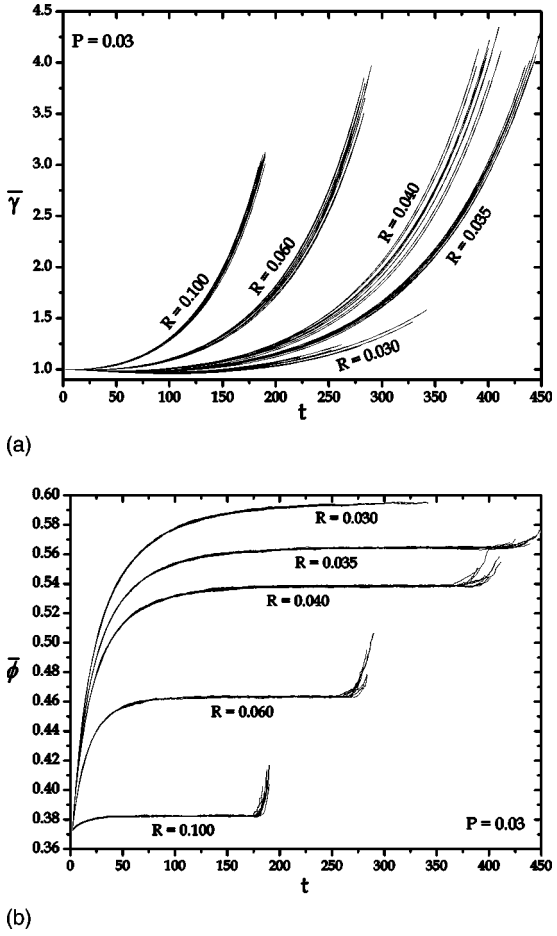

FIG. 6. (a) Mean biofilm thickness and (b) mean porosity values as a function of the dimensionless time.

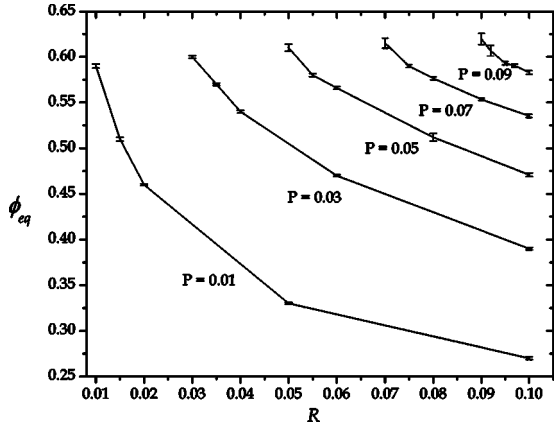

FIG. 7. Equilibrium porosity values for different CA parameters.

Figure 7 shows the mean equilibrium porosity value ϕ_{eq} and standard deviation for different values of R and P. These two estimators were obtained after 20 simulations for each pair R and P with $R \geqslant P$ (when $R<P$ the biofilm is unstable since the probability of death is larger than the probability of birth). The equilibrium porosity value ϕ_{eq} is proportional to P. In the figure it can be observed that a large death probability associated with a large colonization rate gives a narrower porosity range at equilibrium; moreover, for a fixed death rate, increasing the colonization potential reduces porosity at equilibrium (before detachment).

In Fig. 8 the average critical thickness $\overline{\gamma_c}$ in 20 simulations is plotted. Minimal biofilm growth occurs for $P=R$; when R is slightly bigger than P the mean surface increases to a maximum value; after this maximum is reached the behavior is monotonically decreasing for increasing values of R. All of the graphs show that, for each death rate (compe-

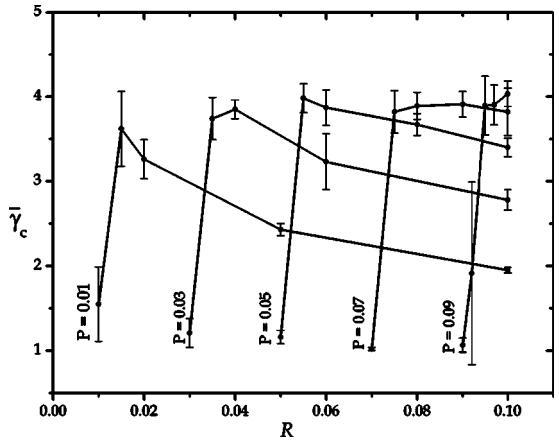

FIG. 8. Dimensionless critical mean thickness as a function of R for different values of P.

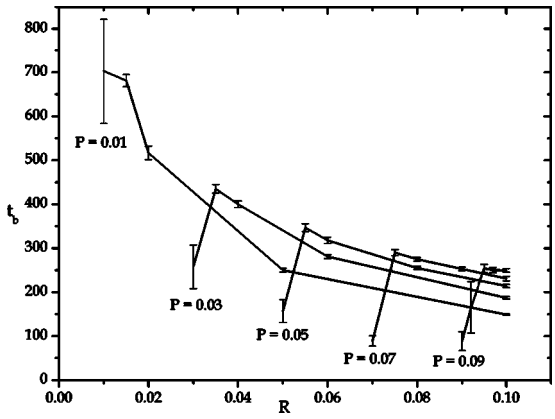

FIG. 9. Biofilm breaking dimensionless time as a function of *R*.

tition strength), there is a critical *R* (colonization strength) where thickness reaches a maximum. Note that the maximum thickness is roughly the same for all *P*. However, as *R* increases beyond the point of maximum thickness the range of variability for critical thickness (that can be seen as a heterogeneity measurement) becomes narrower meaning that for large colonization capability, variability in thickness before detachment is reduced.

The time to reach the breaking condition and its standard deviation as functions of *R* for different values in *P* are shown in Fig. 9. Here again the mean and standard deviation were calculated after 20 simulations. This figure shows that the time needed to reach the breaking condition is inversely proportional to *R* and proportional to *P*. A minimum in the curves is presented when $R=P$ except for $P=0.01$ where the variance is too large to capture this behavior. Note that, roughly, the smaller the death rate *P* is (competition strength), the longer it takes for the biofilm to detach and that, again, for a fixed *P*, increases in colonization capabilities *R* decrease the time to detachment.

VIII. CONCLUDING REMARKS

In a recent paper [32], the development and detachment of biofilms of *Pseudoalteromonas tunicata*, a marine bacterium, was investigated. The paper explored the role that cell death plays in the structure of biofilms. The authors found that this species shows a reproducible pattern of cell death that, in the long term, may play an important role in biofilm dispersion. Dead cells were observed between 48 and 95 h of development of consortia, and regions of extensive killing occurred into the biofilms that induced its detachment. The paper points out that cell death inside biofilms may be a widespread phenomenon of importance for biofilm dispersal but that little is known about the mechanisms by which biofilms with holes within are formed.

In the model we have developed along this work we consider several time and spatial scales to deal with. We have, certainly, disregarded several biofilm components and their associated dynamics as we have mentioned before. The model is built upon two submodels: the fluid dynamics model and the population dynamics submodel. The creation of voids within biofilms is a process that occurs with temporal and spatial organization during biofilm development. In particular, cell death and the creation of voids are important in the detachment process. Our approach is an approximation to the processes of cell death and void creation but we do not explicitly attempt determine the mechanisms that produce the voids since these are still unclear as discussed by Mai-Prochnow *et al.* [32] and Webb *et al.* [33].

We believe our model presents a plausible explanation for the process of biofilm development, the formation of cavities or pores within its structure, and the final detachment process. Our model can reproduce the heterogeneous behavior of a bacterial layer, its rupture, and the surface fingering behavior. We have shown that nutrient distribution depends mainly on biofilm thickness and in a lesser degree on heterogeneities in porosity, tortuosity, and permeability. Through numerical investigation of our model we have found that there exists a critical thickness such that nutrient concentration at the substrate-biofilm interface is not enough to maintain the bacteria alive. At this point, the biofilm begins to lose its mechanical resistance that combined with the fluid drag forces leads to the detachment/rupture processes.

The average porosity shows a transient behavior before an equilibrium value is reached that depends on *R* and *P* as described in the previous section. After this critical point is achieved, porosity rapidly increases until the bacterial layer breaks. The breaking time strongly depends on the parameters *R* and *P*. Heterogeneity plays an important role in this problem, particularly in the breaking times and average surface growth, as shown in Figs. 8 and 9, the dependence is less evident for the mean porosity value, where the standard deviation is small as shown in Fig. 7.

Current research is under way to model multispecies biofilms where the effects of metabolic waste and biocide application over the colony are evaluated as well as drag effects over the growth surface among other things. Needless to say, the fluid dynamics can be improved by considering dispersion processes, including permeability and tortuosity models applicable to bacterial layers.

The model describes the behavior of a two-dimensional biofilm coupling conservation equations and a cellular automaton. Since transport characteristic times are shorter than the mean bacterial life, it was possible to simplify the equations by neglecting temporal derivatives except for the porosity. The numerical grids used to solve the system were designed to satisfy the control volume porous medium definition by assuming that the characteristic bacterial length is very small compared with the continuum control volume. In our model bacterial grid density is larger than the corresponding density for the conservation equations grid.

We must point out that our model does not consider the effect on biofilm dynamics of the EPS. It is known that the EPS plays a role in certain types of antibiotic neutralization and that its mechanical and physical characteristics are important in biofilm constitution and transport of cell signaling, nutrient, biocide, diffusion, and so forth. However, it is also known [3] that, at least in *Pseudomonas aeruginosa*, the expression of the quorum sensing factor HSL although required for the conformation of a biofilm with typical architecture (channels, mushroom structures, and so forth) is not associ-

ated with their ability to resist killing by antibiotics, that is, typical biofilm architecture does not matter that much in this case. So although we are aware that not introducing EPS into our model may make it less general, as far as our objectives are concern, it is a reasonable assumption.

Obviously our breaking condition must also be improved and it must incorporate the mechanical effects of the EPS matrix. However, the scale at which our model works, and the phenomenological nature of its conception, makes it possible to neglect the EPS matrix in this case too. Our main interest has been to study the interactions of biofilm growth with the fluid. The scale at which we have modeled biofilm growth does not involve the mechanical restrictions that the EPS imposes. Bacterial growth is modeled essentially as a random undirected process that depends on the state of local neighborhoods. A more realistic approach would be to consider EPS development and the associated geometric constraints for bacterial growth. This is an ongoing project for which only incipient results exist at the moment.

Donlan [1] review on biofilms observes that to explain biofilm detachment three processes appear to be the most important: erosion or shearing, sloughing, and abrasion. The model presented in this paper addresses the issue of sloughing due to nutrient depletion. As stated by Lewis [3], genes controlling biofilm destruction can be a very important factor for eradication of biofilms. Our model, although in theoretical terms, is able to reproduce breaking/detachment, what amounts to biofilm destruction, under the simple and reasonable hypothesis of postulating a correlation between detachment and nutrient depletion. Assuming the existence of drugs that attack the biofilm self-destruction pathways, this may be the way to go for the efficient eradication of biofilms [3]. We believe our model gives theoretical support for such idea based on simple physical and biological postulates.

Finally, we would like to point out that with our approach it is possible to estimate the dimension of the alive bacterial layer if we assume that dead bacteria are not washed away, but become part of the EPS or biofilm supporting structure, as described in Luna *et al.* [34], where the fraction of living versus dormant or dead bacteria is measured in marine sediments.

ACKNOWLEDGMENTS

Thanks to Rodolfo Suárez whose advice was fundamental for the realization of this work. The work of G.D.Z., C.P.F., and J.X.V.H. was supported by IMP Grant No. D.00154 and of E.L. by IMP Grant No. D.02100.

[1] R. M. Donlan, Emerg. Infect. Dis. **8**, 881 (2002).
[2] P. S. Stewart, M. A. Hamilton, B. Goldstein, and B. T. Schneider, Biotechnol. Bioeng. **49**, 445 (1996).
[3] K. Lewis, Antimicrob. Agents Chemother. **45**, 999 (2001).
[4] S. Pilyugin and P. Waltman, SIAM (Soc. Ind. Appl. Math.) J. Appl. Math. **59**, 1552 (1999).
[5] D. A. Jones and H. Smith, SIAM (Soc. Ind. Appl. Math.) J. Appl. Math. **60**, 1576 (2000).
[6] E. D. Stemmons and H. L. Smith, SIAM (Soc. Ind. Appl. Math.) J. Appl. Math. **61**, 567 (2000).
[7] J. Dockery and I. Klappler, SIAM (Soc. Ind. Appl. Math.) J. Appl. Math. **62** (3), 853 (2001).
[8] D. Jones, H. V. Kojouharov, D. Le, and H. L. Smith, J. Math. Biol. **DOI.10.1007/**, s00285-003-0202-I (2003).
[9] C. M. Bishop and B. E. Rittmann, Water Sci. Technol. **32**, 263 (1996).
[10] O. Wanner and W. Gujer, Biotechnol. Bioeng. **28**, 314 (1986).
[11] C. Picioreanu, M. C. M. van Loosdrecht, and J. J. Heijnen, Biotechnol. Bioeng. **57**, 718 (1998).
[12] C. Picioreanu, M. C. M. van Loosdrecht, and J. J. Heijnen, Biotechnol. Bioeng. **58**, 101 (1998).
[13] C. Picioreanu, M. C. M. van Loosdrecht, and J. J. Heijnen, Biotechnol. Bioeng. **68**, 355 (2000).
[14] C. Picioreanu, M. C. M. van Loosdrecht, and J. J. Heijnen, Biotechnol. Bioeng. **69**, 504 (2000).
[15] C. Picioreanu, M. C. M. van Loosdrecht, and J. J. Heijnen, Biotechnol. Bioeng. **72**, 205 (2001).
[16] H. J. Eberl, D. F. Parker, and M. C. M. van Loosdrecht, Theor Med. **3**, 161 (2001).
[17] S. W. Hermanowicz, U. Schindler, and P. Wilderer, Water Sci. Technol. **32**, 99 (1995).
[18] D. de Beer and P. Stoodley, Water Sci. Technol. **32**, 11 (1995).
[19] R. Islas-Juarez, M. I. thesis, Universidad Nacional Autonoma de Mexico, 2003.
[20] E. L. Cussler, *Diffusion Mass Transfer in Fluid Systems*, 1st ed. (Cambridge University Press, New York, 1997).
[21] C. N. Davies, Proc. Inst. Mech. Eng. **1B**, 185 (1952).
[22] P. M. Adler and J.-F. Thover, Appl. Mech. Rev. **51**, 537 (1998).
[23] A. Padilla *et al.* (unpublished).
[24] C. M. Bender and S. A. Orzag, *Advanced Mathematical Methods for Scientists and Engineers*, International edition (McGraw-Hill, Singapore, 1978), Vol. 1, Chap. 3, p. 62.
[25] H. Horn, H. Reiff, and E. Morgenroth, Biotechnol. Bioeng. **81**, 607 (2003).
[26] L. Mascari *et al.*, Biotechnol. Bioeng. **83**, 65 (2003).
[27] I. Klapper *et al.*, Biotechnol. Bioeng. **80**, 289 (2002).
[28] S. W. Hermanowicz, Math. Biosci. **169**, 1 (2001).
[29] S. W. Hermanowicz, Water Sci. Technol. **39**, 107 (1999).
[30] J. O. Indekeu and G. V. Giuraniuc, Physica A **336**, 14 (2004).
[31] D. G. Allison *et al.*, FEMS Microbiol. Lett. **167**, 179 (1998).
[32] A. Mai-Prochnow *et al.*, Appl. Environ. Microbiol. **70**, 3232 (2004).
[33] J. Webb *et al.*, J. Bacteriol. **185**, 4585 (2003).
[34] G. M. Luna, E. Manini, and R. Danovaro, Appl. Environ. Microbiol. **68**, 3509 (2002).